frontiers in Earth Science

ORIGINAL RESEARCH
published: 14 May 2021
doi: 10.3389/feart.2021.675150

How Does the Arctic Sea Ice Affect the Interannual Variability of Tropical Cyclone Activity Over the Western North Pacific?

Hao Fu[1,2], Ruifen Zhan[2,3], Zhiwei Wu[2,3], Yuqing Wang[4] and Jiuwei Zhao[2,5]*

[1] Shanghai Typhoon Institute of China Meteorological Administration, Shanghai, China, [2] Department of Atmospheric and Oceanic Sciences, Institute of Atmospheric Sciences, Fudan University, Shanghai, China, [3] CMA-FDU Joint Laboratory of Marine Meteorology, Shanghai, China, [4] Department of Atmospheric Sciences, International Pacific Research Center, School of Ocean and Earth Science and Technology, University of Hawaii at Manoa, Honolulu, HI, United States, [5] Division of Environmental Science and Engineering, Pohang University of Science and Technology, Pohang, South Korea

OPEN ACCESS

Edited by:
Wen Chen, Institute of Atmospheric Physics (CAS), China

Reviewed by:
Jingliang Huangfu, Institute of Atmospheric Physics (CAS), China
Pang-chi Hsu, Nanjing University of Information Science and Technology, China

***Correspondence:**
Ruifen Zhan
zhanrf@fudan.edu.cn

Specialty section:
This article was submitted to Atmospheric Science, a section of the journal Frontiers in Earth Science

Received: *02 March 2021*
Accepted: *16 April 2021*
Published: *14 May 2021*

Citation:
Fu H, Zhan R, Wu Z, Wang Y and Zhao J (2021) How Does the Arctic Sea Ice Affect the Interannual Variability of Tropical Cyclone Activity Over the Western North Pacific? Front. Earth Sci. 9:675150. doi: 10.3389/feart.2021.675150

Although many studies have revealed that Arctic sea ice may impose a great impact on the global climate system, including the tropical cyclone (TC) genesis frequency over the western North Pacific (WNP), it is unknown whether the Arctic sea ice could have any significant effects on other aspects of TCs; and if so, what are the involved physical mechanisms. This study investigates the impact of spring (April-May) sea ice concentration (SIC) in the Bering Sea on interannual variability of TC activity in terms of the accumulated cyclone energy (ACE) over the WNP in the TC season (June-September) during 1981–2018. A statistical analysis indicates that the spring SIC in the Bering Sea is negatively correlated with the TC season ACE over the WNP. Further analyses demonstrate that the reduction of the spring SIC can lead to the westward shift and intensification of the Aleutian low, which strengthens the southward cold-air intrusion, increases low clouds, and reduces surface shortwave radiation flux, leading to cold sea surface temperature (SST) anomaly in the Japan Sea and its adjacent regions. This local cloud-radiation-SST feedback induces the persistent increasing cooling in SST (and also the atmosphere above) in the Japan Sea through the TC season. This leads to a strengthening and southward shift of the subtropical westerly jet (SWJ) over the East Asia, followed by an anomalous upper-level anticyclone, low-level cyclonic circulation anomalies, increased convective available potential energy, and reduced vertical wind shear over the tropical WNP. These all are favorable for the increased ACE over the WNP. The opposite is true for the excessive spring SIC. The finding not only has an important implication for seasonal TC forecasts but also suggests a strengthened future TC activity potentially resulting from the rapid decline of Arctic sea ice.

Keywords: tropical cyclones, accumulated cyclone energy, sea ice, Bering Sea, subtropical westerly jet

INTRODUCTION

Tropical cyclone (TC) activity over the western North Pacific (WNP) exhibits strong interannual variability (Wang and Chan, 2002; Chan and Liu, 2004; Camargo and Sobel, 2005; Zhao et al., 2011; Zhan and Wang, 2016). Fox example, TC number over the WNP was notably high in 2015 with 13 category 4–5 TCs, but extremely low in 1999 without any category 4–5 TCs. Therefore, to understand the observed interannual variability of TC activity and the related physical processes has been a topic of great interest in the last decades (Chia and Ropelewski, 2002; Chan and Liu, 2004; Camargo and Sobel, 2005; Chan, 2005; Fan, 2007; Du et al., 2011; Zhan et al., 2011a,b, 2013; Tao et al., 2012; Zhang et al., 2015; Zhan and Wang, 2016; Gao et al., 2018).

Many previous studies have revealed the relationship between El Niño-Southern Oscillation (ENSO), the strongest interannual signal in the tropics, and TC activity over the WNP (Chia and Ropelewski, 2002; Chan and Liu, 2004; Camargo and Sobel, 2005; Chan, 2005; Huangfu et al., 2018, 2019). During the El Niño years, TC genesis location shifts to the southeastern quadrant of the WNP, and most TCs tend to achieve higher intensity due to an increase in their lifetime over the open ocean. A recent study has further shown that stronger ENSO events are likely to have more notable impact on TC activity over the WNP (Zhan et al., 2018). In addition to ENSO, the sea surface temperature (SST) anomalies (SSTA) over the East Indian Ocean (EIO) were shown to play an important role in modulating TC genesis frequency over the WNP (Du et al., 2011; Zhan et al., 2011a,b; Tao et al., 2012). In the years with cold SSTA over the EIO, the genesis frequency of weak TCs is significantly higher than in the years with warm SSTA (Du et al., 2011; Zhan et al., 2011a; Tao et al., 2012) although the EIO SSTA has no significant effect on TC genesis location and the frequency of strong TCs (Zhan et al., 2011a). The SST gradient (SSTG) between the Southwest Pacific and the western Pacific warm pool was found to trigger a cross-equatorial pressure gradient, which exerts a strong influence on the air-sea interaction over the tropical Pacific, greatly modulating WNP TC genesis frequency and intensity over the WNP (Zhan et al., 2013; Zhan and Wang, 2016). More recently, several studies also have suggested that the Pacific Meridional Mode (PMM) can modulate the interannual variation of WNP TC activity, with more and stronger TCs in the positive PMM phase (Zhang et al., 2015; Gao et al., 2018). The modulation of TC activity by the PMM is mainly through the anomalous zonal vertical wind shear (VWS), especially in the southeastern quadrant of the WNP.

In the last decade or so, more and more attentions have been paid to changes in Arctic sea ice because its anomalies may impose a great impact on the global climate system (Royer et al., 1990; Deser and Teng, 2008). The polar amplification–a feature with temperatures warming faster in the Arctic than the rest of the Earth was widely accepted. Namely, the surface temperature at high latitude would affirmatively respond to the change of local sea ice (Barnes, 2013; Screen and Simmonds, 2013). Several studies have found that Arctic temperature anomalies can influence the atmospheric circulation and weather patterns in the Northern Hemisphere (Balmaseda et al., 2010; Rinke et al., 2013; Screen et al., 2013). Both observational and modeling studies manifested that there was a link between atmospheric circulations at lower latitude and Arctic temperature/sea ice, but the corresponding mechanism of atmospheric circulation response at lower latitude remained uncertain. For example, some studies revealed that the rise of Arctic temperature would reduce the equator-to-pole surface temperature gradient, and then weaken the mid-latitude westerly jets (Schneider et al., 2014; Screen, 2014). However, Wu et al. (2016) found that the decrease in Arctic sea ice sustaining from winter to next spring would accelerate the East Asian subtropical westerly jet (SWJ), a narrow-and-fast westerly band extending from Asia to the North Pacific in the upper-troposphere during boreal summer, by triggering a Rossby wave train. Smith et al. (2017) also showed that a local low pressure anomaly induced by Arctic warming could strengthen the mid-latitude westerlies. In fact, compared with the background circulation, the remote impact of Arctic sea ice on the lower-latitude circulation is more likely to be important (Walsh, 2014; Woolings et al., 2014).

Several studies found a negative correlation between sea ice concentration (SIC) in the Okhotsk Sea from preceding winter to spring and the annual TC frequency in the TC season over the WNP (Fan, 2007; Fan and Wang, 2009). Fan and Wang (2009) thus introduced the winter sea ice index as a predictor to a statistical forecast model for seasonal TC genesis frequency over the WNP and showed good prediction skill. They attributed the relationship between the SIC and the TC genesis frequency to the North Pacific Oscillation (NPO) triggered by the SIC in spring, which led to the dynamic and thermodynamic condition changes over the WNP maintaining from spring to the TC season by a teleconnection wave train. Since Arctic sea ice has a strong impact on the global climate system and shows a significant influence on TC genesis frequency over the WNP, a natural question arises as to whether Arctic sea ice could have any significant effects on other aspects of WNP TCs, such as TC intensity, lifespan, and track; and if so, what are the involved physical mechanisms. In addition, previous studies have shown that the SWJ plays an important role in affecting the weather and climate over East Asia and the WNP (Liang and Wang, 1998; Zhao et al., 2015). The SWJ can also affect TC activity, including genesis, structure and intensity changes, and even TC extratropical transition (Park et al., 2009; Cowan and Hart, 2020). Since the anomalous Arctic sea ice would exhibit an important influence on the SWJ (Wu et al., 2016), the Arctic sea ice might modulate TC activity over the WNP through affecting the SWJ.

Different from Fan (2007), who focused on the relationship between TC genesis frequency and the Arctic sea ice in the Okhotsk Sea, in this study, we focus on how the Arctic sea ice in the Bering Sea in spring affects the interannual variability of TC activity over the WNP in terms of the accumulated cyclone energy (ACE), which reflects not only TC genesis frequency but also the prevailing TC tracks, intensity, and lifetime (Bell et al., 2000; Camargo and Barnston, 2009; Kim et al., 2013; Zhan and Wang, 2016). We found that the spring SIC anomaly has a significant impact on the interannual variability of TC ACE over the WNP in the TC season with higher/lower ACE in response to the reduced/increased spring SIC. We will show that the spring

SIC triggers a cloud-radiation-SST feedback in the Japan Sea and its adjacent regions, inducing large-scale conditions over East Asia and the WNP and significantly affecting TC activity over the WNP. The remainder of the paper is organized as follows. Section "Data and Methodology" describes the datasets and analysis methods used in this study. The statistical relationship between Artic sea ice and TC ACE over the WNP is examined in Section "Results From Statistical and Regression Analyses." The possible mechanisms are elucidated in Section "Possible Mechanisms" based on both diagnostic analyses and climate model sensitivity experiments. Major conclusions are summarized and discussed in the last section.

DATA AND METHODOLOGY

All TC statistics were based on the 6-hourly TC best-track data for the WNP during 1981–2018 from the Joint Typhoon Warning Center (JTWC). To minimize subjectivity in the identification of weak systems, we focused on TCs with maximum sustained 10-m wind speed larger than 35 knots. The result from the calculated monthly correlation between the spring SCI and ACE shows that the spring SIC has relatively low negative correlation with October and November ACE over the WNP, suggesting that the influence of the spring SIC could last until September. Thus, in this study, the TC season was defined from June to September (JJAS) each year.

Several integrated TC metrics have been used to represent TC activity, such as the number of intense TCs, TC days, the power dissipation index (PDI) – a measure of the accumulated wind power destructiveness of all TCs (Emanuel, 2005), and the ACE – an integrated measure of TC activity (Bell et al., 2000). Since TC activity includes not only genesis frequency but also prevailing tracks, intensity, and lifetime, an integrated variable is better to represent various aspects of TC activity. In this study, we used ACE as the measure of the overall TC activity, which is defined as the sum of the square of the maximum sustained 10-m wind speed at 6-h intervals for all TCs over the WNP in the TC season of each year, with its basic unit of 10^5 m^2 s^{-2}. To analyze the spatial ACE distribution, we divided the WNP basin (0°–40°N, 100°–180°E) into grid boxes of 5° longitudes × 5° latitudes and calculated the sum of the square of the maximum sustained 10-m wind speed for all TCs passing each grid box.

The monthly SIC and SST data at 1° longitude × 1° latitude grids were derived from the Hadley Center Sea Ice and Sea Surface Temperature dataset (HadISST) (Rayner et al., 2003). Since the SIC in the Bering Sea in April-May exhibits the higher correlation with the ACE over the WNP in the TC season than that in March-May, we mainly examined the SIC in spring (April-May) as a potential preceding signal. The monthly mean atmospheric data at 0.25° longitude × 0.25° latitude grids were obtained from the ECMWF (European Center for Medium-Range Weather Forecasts)'s fifth generation reanalysis (ERA5; Hersbach et al., 2020).

Five indices were defined in this study based on our following analyses. Two Arctic sea ice indices were defined as the SIC anomalies averaged, respectively, in the eastern region over the Bering Sea (178°E–160°W, 57°–68°N) and the western region over the Barents Sea (27°–65°E, 67°–80°N) based on **Figure 1**. Two SST indices were defined as the SST anomalies averaged, respectively, in the Japan Sea (30–50°N,128°–150°E) and the tropical central Pacific (CP, 160°E–160°W, 0°–20°N) based on **Figure 6**. Note that here the Japan Sea is referred to the region including both the Japan Sea and its adjacent regions for the convenience of following discussion. The last index is the SWJ index, which was defined as the zonal wind at 200-hPa averaged in the region of 30°–45°N, 130°–180°E. All data and indices were linearly detrended before further analysis since we focused on the interannual variability in this study.

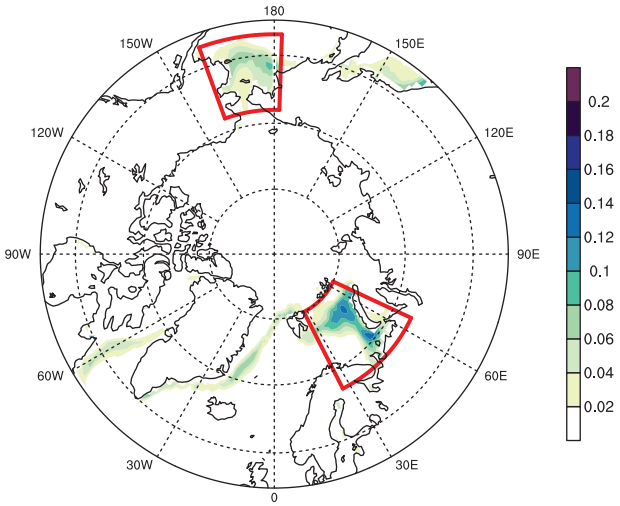

FIGURE 1 | Spatial distribution of standard deviations of sea ice concentration (shaded; %) north of 55°N in spring (April-May). The red boxes indicate the regions of Bering Sea (178°E–160°W, 57°–68°N) and Barents Sea (27°–65°E, 67°–80°N), respectively.

The algorithm of Ashok et al. (2003) was used to subtract the effect of factor A from another factor B, which has the following form:

$$I_{RB} = I_B - r(I_B, I_A)\mathrm{O}'\tilde{I}_A, \tag{1}$$

where I_A is index of A, and $\tilde{I}_A$ denotes the normalized I_A. O′ was the standard deviation of index of B (I_B), while $r(I_B,I_A)$ stands for the correlation coefficient between index A and index B. The term I_{RB} on the left-hand side is the net signal of index B without the signal of index A.

In addition, following Murakami et al. (2014), we quantified the relative contributions to the interannual variability of ACE by TC genesis frequency, track, intensity, and the non-linearity of the first three factors. The climatological mean of ACE in a specific grid box A can be written as:

$$\overline{f(A)} = \iint_C \overline{g(A_0)}\,\overline{t(A,A_0)}\,\overline{v^2(A,A_0)}dA_0, \tag{2}$$

where f(A) is the ACE in a specific grid box A; an overbar indicates the climatological mean; g(A_0) is the TC genesis frequency in the grid box A_0; and t(A, A_0) is the probability for

a TC formed in the grid box A_0 to travel into the grid box A. $v^2(A, A_0)$ stands for the mean square of maximum wind speed for TCs in the grid box A and formed in grid box A_0; and C is the entire integration domain. For the period 1981–2018, the ACE anomalies relative to the climatological mean in the grid box A can be expressed as:

$$f'(A) = \iint_c g'(A_0)\overline{t(A, A_0)}\overline{v^2(A, A_0)}dA_0 + \iint_c \overline{g(A_0)}t'(A, A_0)\overline{v^2(A, A_0)}dA_0 + \iint_c \overline{g(A_0)}\,\overline{t(A, A_0)}v^{2\prime}(A, A_0)dA_0 + NL, \quad (3)$$

where the prime indicates the corresponding anomaly. Eq. (3) can quantify the contribution of each factor to the total ACE anomaly in each given grid box. The terms on the right-hand side represent the contributions by TC genesis frequency anomaly (first term), track density anomaly (second term), intensity anomaly (third term), and the nonlinear effect (fourth term), respectively. The non-linear term is calculated as:

$$NL = \iint_c g'(A_0)t'(A, A_0)\overline{v^2(A, A_0)}dA_0 + \iint_c \overline{g(A_0)}t'(A, A_0)v^{2\prime}(A, A_0)dA_0 + \iint_c g'(A_0)\overline{t(A, A_0)}v^{2\prime}(A, A_0)dA_0 + \iint_c g'(A_0)t'(A, A_0)v^{2\prime}(A, A_0)dA_0, \quad (4)$$

The fourth-generation atmospheric general circulation model (AGCM) developed at the Max Planck Institute (Roeckner et al., 1996), named ECHAM4, was used to conduct sensitivity experiments to examine the response of the large-scale atmospheric circulation to the SST anomalies over the Japan Sea. The prognostic variables of the model were expressed by truncated series of spherical harmonics in the horizontal at truncation T42 and by the finite-differencing in the hybrid σ–pressure coordinate in the vertical with 19 uneven vertical levels. A semi-implicit time-differencing scheme was used for model time integration. The model physics include the surface turbulent fluxes calculated based on the Monin–Obukhov similarity theory, the horizontal diffusion in a hyper-Laplacian form, the ECMWF longwave and shortwave radiation schemes, and the convective parameterization scheme documented in Nordeng (1994). More details about the model can be found in Roeckner et al. (1996).

RESULTS FROM STATISTICAL AND REGRESSION ANALYSES

Correlations Between the SIC and the ACE Over the WNP

To determine the key area of the seasonal SIC variability, we calculated the standard deviation of the interannual variability of the spring SIC anomalies in the high latitudes of the Northern Hemisphere with the spatial distribution shown in **Figure 1**.

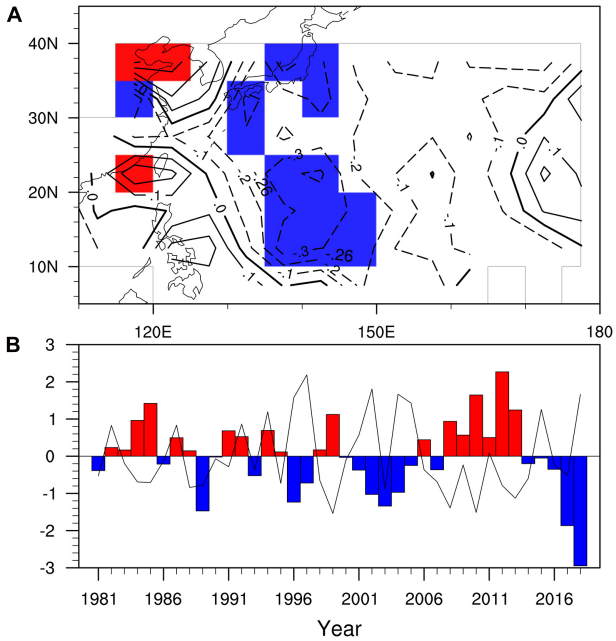

FIGURE 2 | The relationship between the WNP ACE in the TC season and the spring SIC in Bering Sea during 1981–2018. **(A)** Correlation coefficients between them; **(B)** normalized time series of ACE (line; averaged in the region of 130°–160°E, 0°–40°N) and the spring SIC index in the Bering Sea (bar). In panel **(A)**, the shaded areas in blue (red) indicate the negative (positive) correlation significant at 90% confidence level.

Large spring SIC variability is mainly located in the Bering Sea and the Barents Sea, followed by some small variability in the northern Sea of Okhotsk and on the western and eastern sides of the Greenland. To quantitatively measure the SIC variability, two SIC indices with large variability were defined as introduced in Section "Data and Methodology:" one with the spring SIC anomalies averaged in the Bering Sea and the other averaged in the Barents Sea. We calculated the correlations between the ACE over the WNP in the TC season with the above two spring SIC indices, respectively. The results showed that the ACE has a significant negative correlation with the spring SIC in the Bering Sea, but the correlation with the spring SIC in the Barents Sea is not statistically significant. Therefore, we focused on the influence of the spring SIC in the Bering Sea on the ACE over the WNP in this study. We will refer to the spring SIC over the Bering Sea simply as the spring SIC in our following discussion for convenience without any ambiguity.

Figure 2A shows the spatial distribution of correlation coefficients between the spring SIC and ACE over the WNP in the TC season. As we can see, although some scattered positive correlations appeared in the southern East China Sea, the northern Yellow Sea, and east of 170°E of the WNP, the correlation coefficients between the spring SIC and ACE over the WNP in the TC season were generally negative with significant correlations between 130°E and 150°E, with the *p*-Value less than 0.1. We further defined the ACE averaged in the region (130°E–160°E, 0–40°N) as an overall ACE index in the WNP basin.

TABLE 1 | Correlation matrix among spring SIC index, SST indices in the Japan Sea in spring and the TC season (T-season), SWJ index, and ACE during 1981–2018.

	SIC (spring)	SST in Japan Sea (spring)	SST in Japan Sea (T-season)	SWJ (T-season)	ACE (T-season)
SIC (spring)	1	−0.16	**–0.38**	**–0.31**	**–0.47**
SST in Japan Sea (spring)		1	0.18	0.27	0.1
SST in Japan Sea (T-season)			1	**–0.44**	−0.19
SWJ				1	**0.34**
ACE					1

The significant coefficients at the 95% confidence level are in bold.

Figure 2B shows the normalized time series of the ACE index in the TC season and the spring SIC index during 1981–2018. Consistent with the result in **Figure 2A**, the ACE and the spring SIC are highly correlated with a correlation coefficient of −0.47 (**Table 1**), which is statistically significant above 99% confidence level. This suggests that the spring SIC most likely have a significant effect on the interannual variability of ACE over the WNP, with higher (lower) ACE over the WNP in response to the decreased (increased) spring SIC in the Bering Sea.

As mentioned above, ACE is an integrated variable including contributions by TC genesis frequency, prevailing tracks, intensity, and lifetime. To better understand the impact of the SIC on TC activity, we calculated the correlations between the SIC index and the three aspects of ACE including TC genesis frequency, track density, and intensity. The correlation coefficients are -0.26, -0.37, and -0.39, for TC genesis, track density, and intensity, respectively. The first one is statistically significant at 90% confidence level, while the other two are significant above 95% confidence level. This suggests that the spring SIC has a significant influence not only on TC genesis frequency, but also on TC tracks and intensity. Further, we examined the individual contributions of TC genesis frequency, tracks, intensity, and the nonlinear effect in Eq. (3) to the variability in ACE averaged in the region (0°–40°N, 130°–160°E) with the results shown in **Figure 3**. Among the four factors, the TC track has the largest contribution to the ACE (nearly 45%), and TC genesis frequency and intensity are the second and third significant contributors, respectively. In contrast, the nonlinear effect is negative and small compared to other terms. This indicates that the spring SIC plays an important role in modulating TC genesis frequency, intensity, and tracks in the TC season over the WNP. Especially, the spring SIC can greatly affect TC tracks. Note that TC tracks in the region north of 20°N show larger contribution than that south of 20°N (figure not shown), suggesting that the reduced (increased) spring SIC is favorable (unfavorable) for the northward shift of TC activity over the WNP.

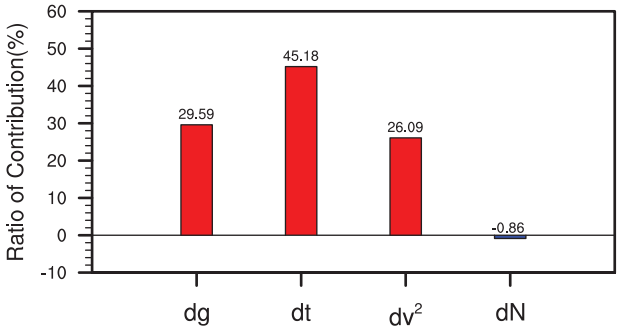

FIGURE 3 | The contributions of TC genesis (dg), TC track (dt), TC intensity (dv^2), and the nonlinear effect (dN) to the ACE averaged in the region (0°–40°N, 130°–160°E) calculated using Eq. (3).

Large-Scale Circulation Response Over the WNP in the TC Season

Since the ACE in the WNP TC season is negatively correlated with the spring SIC in the Bering Sea, it is expected that the large-scale thermodynamic and dynamic conditions closely associated with TC activity over the WNP in the TC season should be also correlated with the spring SIC in the Bering Sea. To confirm this consistency, we have done regression analyses for various dynamic and thermodynamic factors in the TC season over the WNP with respect to the spring SIC during 1981–2018.

Figure 4 shows the regressed 850-hPa winds, 850-hPa relative vorticity, convective available potential energy (CAPE), vertical wind shear between 200 and 850 hPa (VWS), and mass-weighted mean steering flow between 850 and 300 hPa in the TC season over the WNP in response to the negative spring SIC anomaly during 1981–2018. Namely, the SIC index was multiplied by −1 to represent atmospheric response to the reduced SIC (namely the negative SIC anomaly). As we can see from **Figure 4**, in response to the reduced SIC, a number of significant changes occur, including low-level anomalous westerlies over the tropical western Pacific and a tripole-pattern circulation over the WNP with two anomalous cyclones, respectively, in the tropical WNP south of 25°N and east of the Japan Sea, with an anomalous anticyclone in between; an increase in the low-level cyclonic vorticity and the CAPE, and the decrease in VWS over the tropical WNP between 10°N and 30°N. All these responses are favorable for convective activity and TC genesis and intensification in the main TC activity region over the WNP (Weisman and Klemp, 1982; Emanuel, 1994; Rasmussen and Blanchard, 1998). In contrast to the anomalous low-level circulation that are favorable for TC activity in the tropical and subtropical WNP, the response of both CAPE and VWS to the reduced SIC seems to suppress TC activity near the Japan Sea. However, the anomalous northward steering flow north of 30°N around Japan is conducive to more TCs approaching Japan (**Figure 4E**). This is consistent with a significant but weak negative correlation of the ACE in the TC season with the spring

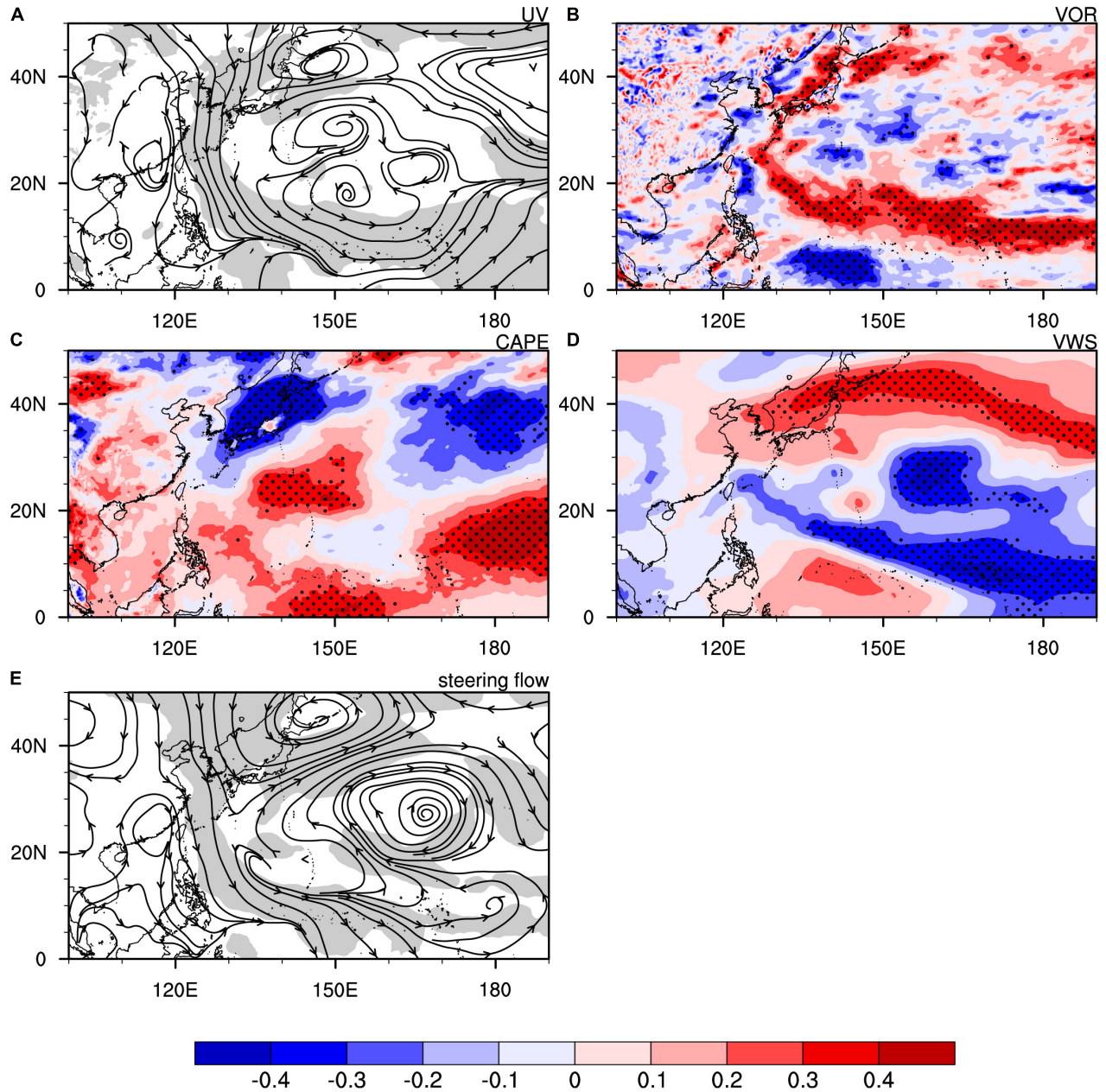

FIGURE 4 | Regressed **(A)** wind field (m s^{-1}) at 850 hPa, **(B)** relative vorticity (10^{-6} s^{-1}) at 850 hPa, **(C)** CAPE (10^{-2} J kg^{-1}), **(D)** vertical wind shear (m s^{-1}) between 200 and 850 hPa, and **(E)** mass-weighted steering flow between 850 and 300 hPa (m s^{-1}) in the TC season with respect to the negative spring SIC index during 1981–2018. Gray shaded in panels **(A,E)** and stippling in panels **(B-D)** denote regions where the regressions are statistically significant above 90% confidence level based on the Student *t*-test.

SIC there (**Figure 2A**). In addition, the anomalous northerly and negative low-level vorticity from the Korean Peninsula to east of the Philippines between 115°E and 130°E in response to the reduced spring SIC are generally unfavorable for TC genesis and intensification. This is also consistent with the positive correlation between the spring SIC and the ACE in the region in the TC season (**Figure 2A**).

Since the upper-tropospheric circulation may play some important roles in TC activity (e.g., Bracken and Bosart, 2000; Fischer et al., 2017), we also examined the regressed 300-hPa temperature, 200-hPa horizontal winds, and 200-hPa zonal winds in the TC season with respect to the spring reduced SIC, with the results shown in **Figure 5**. For a comparison, the climatological mean 200-hPa zonal wind field is also given in **Figure 5B**. In response to the reduced SIC, a significant upper-level cold anomaly appears over the Japan Sea and strong warm anomalies appear over the tropical Pacific (**Figure 5A**), which are consistent with the pattern of the regressed SST anomalies

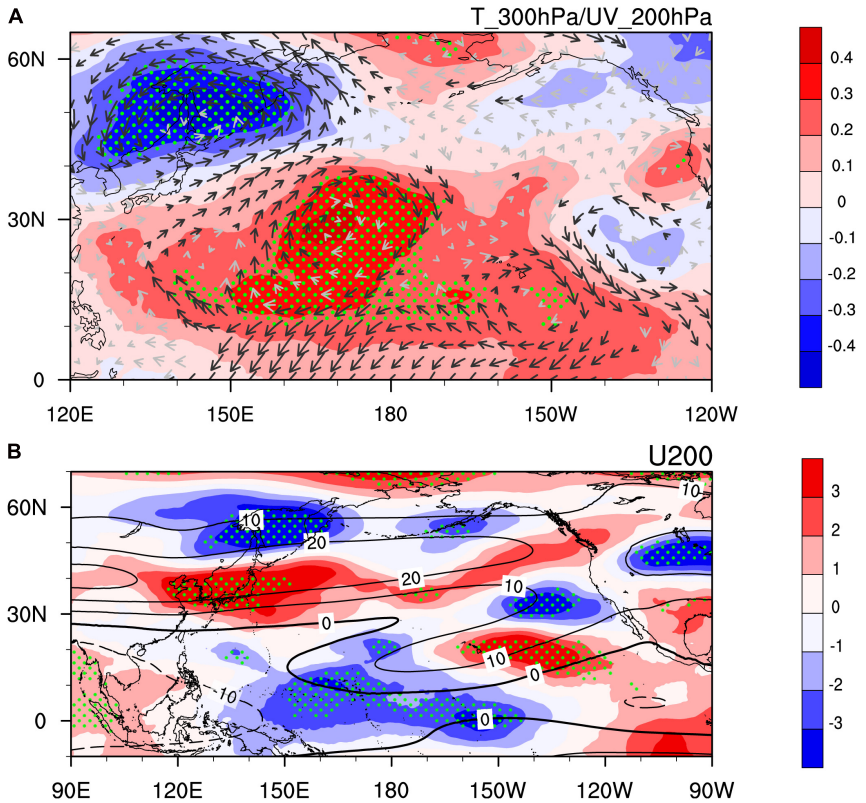

FIGURE 5 | Regressed **(A)** 300-hPa temperature (shaded; K) and 200-hPa wind field (m s^{-1}), and **(B)** 200-hPa zonal wind (shaded; m s^{-1}) in the TC season with respect to the negative spring SIC index during 1981–2018. The black arrows in panel **(A)** and the dots in panels **(A,B)** denote the areas where the regressions are statistically significant above 90% confidence level based on the Student *t*-test. The contours in panel **(B)** denote the climatological mean zonal wind at 200 hPa (U200).

(figure not shown). Corresponding to the above temperature anomaly pattern are an anomalous cyclone over the Japan Sea and an anomalous anticyclone over the tropical WNP (**Figure 5A**) together with a strengthened and southward shifted SWJ in the upper troposphere (**Figure 5B**). These anomalies can be inferred from the thermal wind balance because of the increased meridional temperature gradient (**Figure 5A**).

Previous studies have shown that the anticyclonic circulation south of the SWJ entrance region can dynamically force ascending motion, promote moist convection, and thus favorable for TC development and intensification (Moore and Vanknowe, 1992; Cowan and Hart, 2020). Corresponding to the strengthened and southward shifted SWJ (**Figure 5B**) is an anomalous anticyclonic circulation in the upper troposphere (**Figure 5A**) and increased CAPE (**Figure 4C**) over the tropical and subtropical WNP. Furthermore, we calculated the correlation between the SWJ index and ACE index in the TC season. The correlation coefficient between the two indices reaches 0.34, which is statistically significant at the 95% confidence level (**Table 1**). Therefore, this strongly suggests that the spring SIC can significantly modulate the SWJ over East Asia and the WNP throughout the summer, affecting the large-scale dynamic and thermodynamic atmospheric conditions over the WNP and thus TC activity in the TC season.

POSSIBLE MECHANISMS

In the last section, we have shown that the large-scale circulation response to the spring SIC anomaly in the Bering Sea is consistent with the correlation of the ACE over the WNP in the TC season with the spring SIC. A question arises as to how the spring SIC anomaly can impose a delayed impact on TC activity over the WNP in the TC season because the direct influence of the SIC often weakens quickly in the coming summer. Since the memory of the atmosphere is relatively short, often less than a month (see a review by Zhan et al., 2012), and the ocean has a much longer memory than the atmosphere, we hypothesize that the ocean response to the spring SIC anomaly and the subsequent ocean-atmospheric interaction may play a key bridging role in the connection between the spring SIC in the Bering Sea and the TC activity over the WNP. As we mentioned above, the SST anomalies and the upper-tropospheric air temperature anomalies over the WNP in the TC season show similar spatial patterns in response to the spring SIC in the Bering Sea. According to the thermal wind balance, the southward horizontal temperature gradient can lead to an increase of westerlies with height. This means that the deep air temperature response in the WNP and the strengthening and southward shift of the SWJ are dynamically balanced. Since the SWJ plays an important role in affecting the

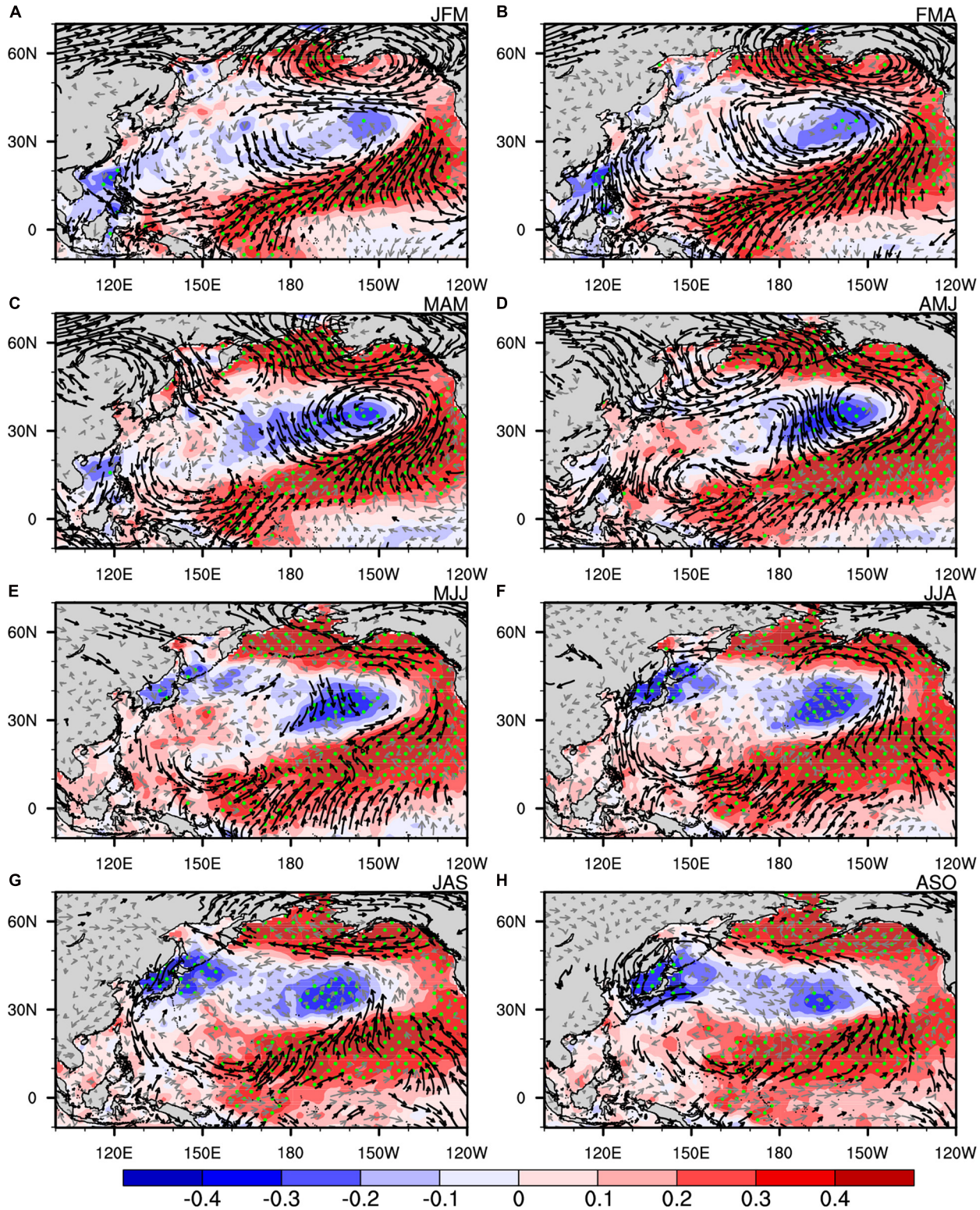

FIGURE 6 | Regressed 3-month moving averaged SST (shaded; °C) and 850-hPa wind (vectors; m s^{-1}) fields with respect to the negative spring SIC index from March to October. **(A)** January-March (JFM); **(B)** February-April (FMA); **(C)** March-May (MAM); **(D)** April-June (AMJ); **(E)** May-July (MJJ); **(F)** June-August (JJA); **(G)** July-September (JAS); **(H)** August-October (ASO). The black arrows denote the wind fields significant at 90% confidence level. The dots denote the areas where the regressions in SST are significant at 90% confidence level.

WNP thermodynamic and dynamic conditions controlling TC activity in the TC season over the WNP, it is key to understand how the spring SIC causes the SST anomaly pattern over the WNP and how the SST anomaly pattern persists through the TC season. Therefore, in this section we explore the possible physical mechanisms by which the spring SIC anomaly contributes to the development and maintenance of the SST anomaly pattern, and affecting the SWJ and thus the TC activity over the WNP in the TC season.

Figure 6 shows the regressed 3-month moving averaged SST and 850-hPa wind fields with respect to the negative SIC index from March to October. A significant change in the regressed SST field is found in the Japan Sea with a gradually enhanced cooling from March-May to August-October, while changes in SST anomalies in other regions remain small in all seasons. We further calculated the correlation between the SST index in the Japan Sea and the spring SIC index in the Bering Sea defined in Section "Data and Methodology". As shown in **Table 1**, this insignificant ($r = -0.16$) correlation in spring turned to significant ($r = -0.38$) at the 95% confidence level in the TC season. This suggests that the reduced spring SIC induces the cooling in the Japan Sea, and the cooling can intensify and maintain through the whole TC season. Note that the cold SST anomaly (and also the cold atmospheric temperature anomaly above) in the Japan Sea associated with the spring SIC is located just to the north of the SWJ (**Figures 5**, **6**). The correlation coefficients between the SWJ index in the TC season and the spring SIC and between the SWJ index and the SST index in the Japan Sea in the TC season are -0.31 and -0.44, respectively, both statistically significant at the 95% confidence level (**Table 1**). This indicates that the SST cooling over the Japan Sea induced by the reduced spring SIC can enhance the climatological meridional atmospheric temperature gradient and thus accelerate the SWJ above.

The possible role of the Japan Sea SST in affecting the SWJ in the TC season can be confirmed by regressing the 200-hPa winds with respect to the negative SST index in the Japan Sea in the TC season without and with the CP SST signal removed using Eq. (1), as shown in **Figure 7**. Note that the regressed SST field with respect to the negative SIC index shows the cold Japan Sea and warm CP anomalies (**Figure 6**). Therefore, removing the CP SST signal is to avoid its significant effect on TC activity over the WNP (Chen and Tam, 2010) and thus to isolate the primary effect of the SST anomaly over the Japan Sea. As expected, the negative Japan Sea SST anomaly with the CP SST anomaly signal retained induces remarkable anomalous westerlies between 30 and 40°N from 100°E to 180°E and an anomalous anticyclonic circulation in the upper troposphere south of 30°N over the tropical WNP (**Figure 7A**). Such a pattern tends to strengthen the SWJ and provide large-scale environmental conditions favorable for TC activity. This is generally consistent with the atmospheric response to the negative spring SIC as shown in **Figure 5**. With the CP SST anomaly signal removed, the anomalous westerlies and anticyclonic circulation in response to the cold Japan Sea anomaly are still significant and similar to those with the CP signal retained although the anomalous anticyclone becomes slightly weaker (**Figure 7B**). Namely, the SST anomaly over the Japan Sea contributes significantly to the SWJ and thus the TC activity over the WNP.

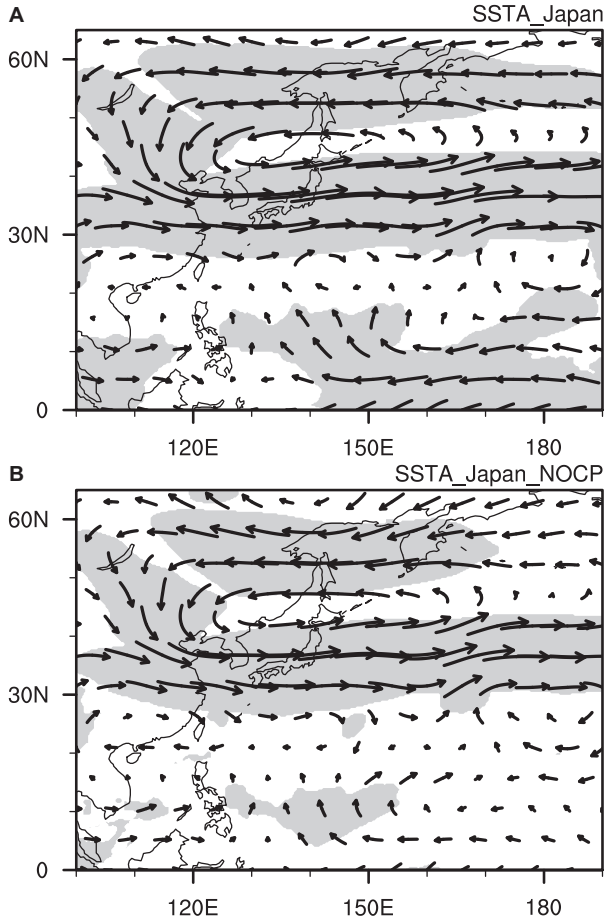

FIGURE 7 | Regressed 200-hPa wind field (m s^{-1}) in the TC season with respect to the negative SST anomaly in the Japan Sea based on panels **(A)** the original data and **(B)** with the CP SST signal removed during 1981–2018. The shaded areas denote where the regressions are statistically significant above 90% confidence level based on the Student *t*-test.

To confirm the above data analysis, we conducted three numerical experiments using the ECHAM4 as briefly described in Section "Data and Methodology". These experiments were designed to demonstrate the independent impact of the Japan Sea SST anomaly on the SWJ in the TC season. The control run was performed with the observed monthly mean climatological SST averaged in the period 1981–2018. The two sensitivity experiments (cold and warm runs) were identical to the control run except that 1°C was subtracted from and added to, respectively, the SST in the Japan Sea as shown in **Figure 8A** from June to September, namely through the TC season. The model was integrated for 30 years for each experiment and the last 25 years were used in the analysis here. The control run generally reproduces reasonably well the observed wind fields at both 850 hPa and 200 hPa (not shown). **Figures 8B–D** show the differences in the simulated 300-hPa temperature and 850-hPa and 200-hPa winds in the TC season between the cold and

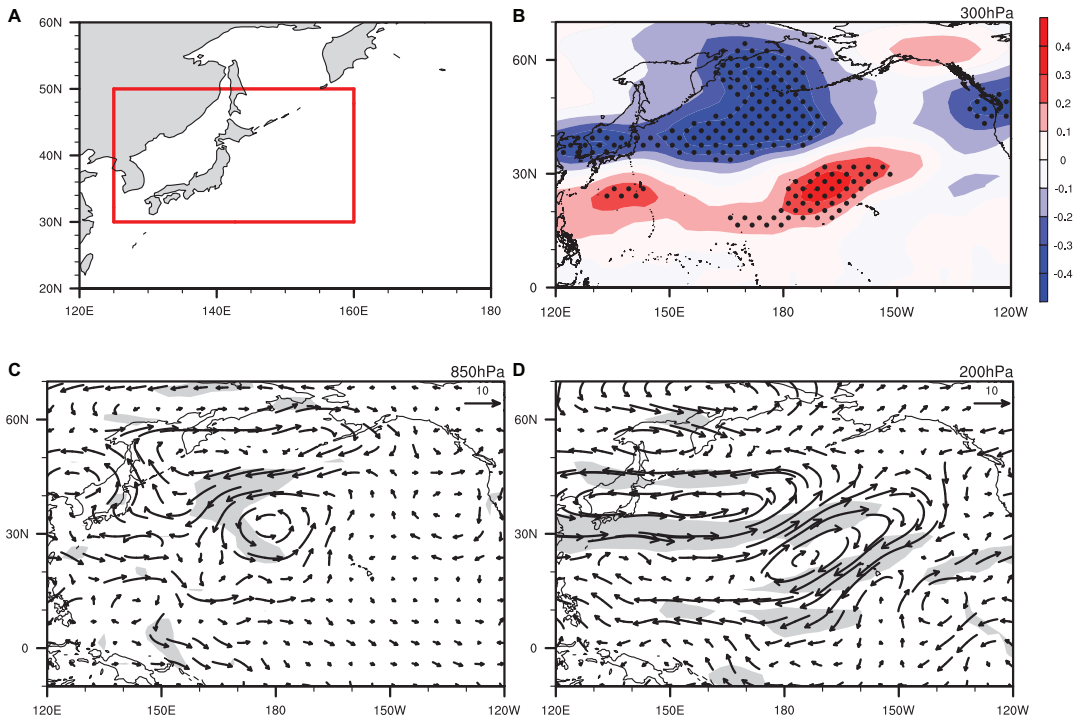

FIGURE 8 | (A) The domain in which SST is modified in the sensitivity experiments. **(B-D)** The differences in the simulated **(B)** 300-hPa temperature (shaded, K), **(C)** 850-hPa, and **(D)** 200-hPa winds (vector; m s^{-1}) between the cold and warm runs based on the ECHAM4 model. The dots in panel **(B)** and the shaded in panels **(C,D)** denote areas where the differences are statistically significant above 90% confidence level based on the Student *t*-test.

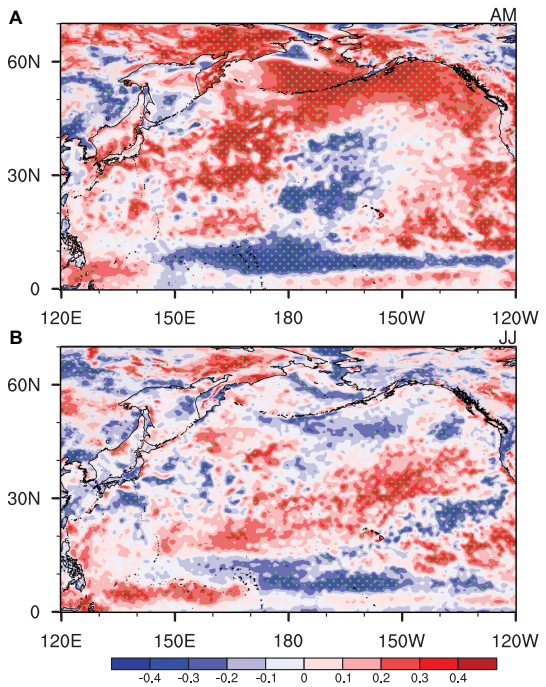

FIGURE 9 | Regressed sensible heat flux (W m^{-2}) averaged in panels **(A)** April-May and **(B)** June-July with respect to the negative spring SIC index. The dots denote the areas where the regressions in sensible heat flux are significant at 90% confidence level.

warm runs. Consistent with the regression analysis shown in **Figure 7**, the simulated differences in 200-hPa winds between the cold and warm SST anomalies over the Japan Sea (**Figure 8D**) show significant westerly anomalies near 30°N from 120° to 180°E and an anomalous anticyclonic circulation south of 30°N over the WNP. At the same time, the difference in the simulated temperature at 300 hPa exhibits a significant cold anomaly to the north and a warm anomaly to the south of 30°N over the WNP (**Figure 8B**), similar to that observed as shown in **Figure 5A**. This suggests that the cold SST in the Japan Sea can indeed lead to the strengthening and southward shift of the SWJ. In addition, the simulated difference in 850-hPa winds between the cold and warm runs (**Figure 8C**) is characterized by an anomalous cyclonic circulation over the tropical WNP, which is favorable for TC activity over the WNP, although the low-level circulation response to the cold Japan Sea is slightly north of that regressed with respect to the spring SIC anomaly (**Figure 4A**). These results confirm the role of Japan Sea SST anomaly in modulating the SWJ and the large-scale environmental conditions affecting the ACE in the TC season over the WNP.

As discussed above, there is a gradually increasing cooling in the Japan Sea from March-May to August-October in response to the spring SIC anomaly (**Figure 6**). Therefore, it is important to understand how the spring SIC anomaly leads to the continuous cooling in the Japan Sea through the TC season. In January-March, the Bering Sea and the Gulf of Alaska is covered by a strong anticyclonic anomaly (**Figures 6A,B**). As the SIC decreases in spring, a cyclonic anomaly over the

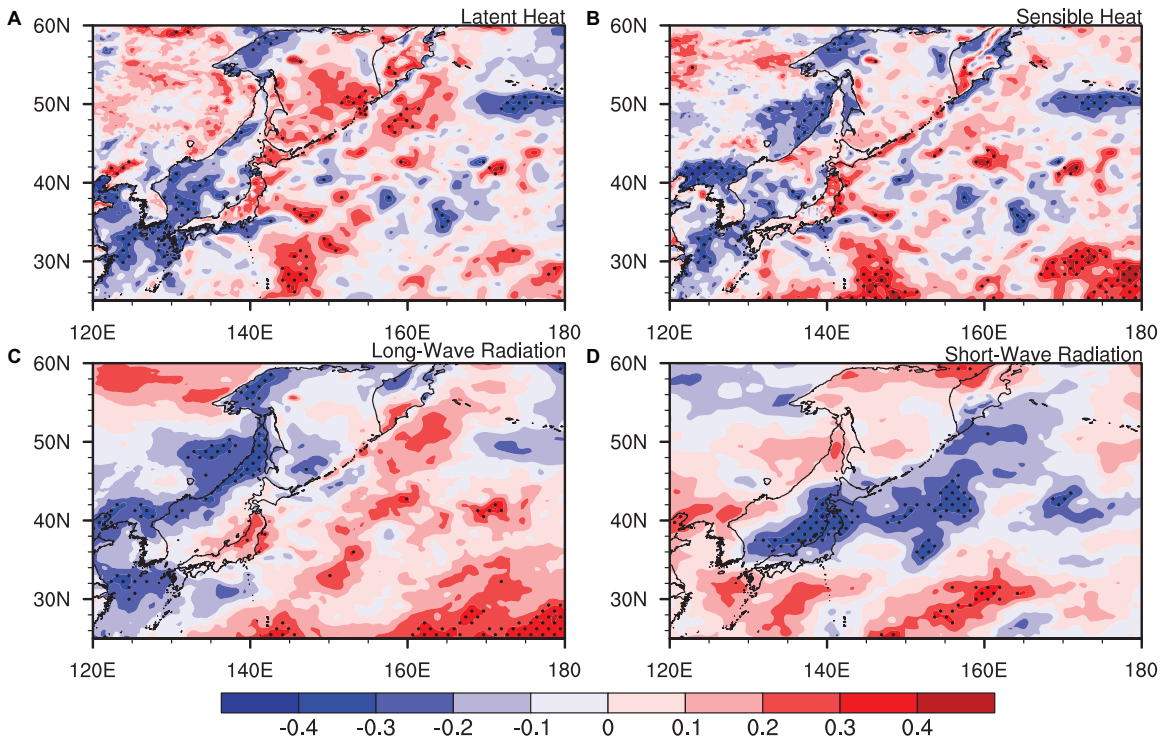

FIGURE 10 | Regressed **(A)** latent heat flux, **(B)** sensible heat flux, **(C)** longwave radiation flux, and **(D)** shortwave radiation flux (W m^{-2}) in the TC season with respect to the negative spring SIC index during 1981–2018. The dotted areas denote where the regressions are statistically significant above 90% confidence level based on the Student *t*-test.

western Bering Sea gradually strengthens and expands around, which contributes to the westward shift and intensification of the Aleutian low (**Figures 6C,D**). Afterwards, the cyclonic anomaly weakens and decays in summer (**Figures 6E,F**). In response to the reduced spring SIC, sensible heat flux over the Bering Sea also exhibits significant positive anomaly in spring, while the positive anomaly rapidly weakens and decays in the coming summer (**Figure 9**). This suggests that the reduced spring SIC significantly modulates the Aleutian low by warming the low-level atmosphere. Meanwhile, the strengthened Aleutian low enhances the northwesterly over the mid-latitude Asian continent, leading to cold continental air intrusion into the Japan Sea and thus the cooling in the Japan Sea by promoting sea surface sensible and latent heat fluxes. However, although the cold air intrusion induced by the spring SIC weakens rapidly from spring to summer, the cooling in the Japan Sea continues through the TC season. This suggests that the reduced SIC in spring triggers the initial cold SST anomaly in the Japan Sea, but the strengthening of the cold SST anomaly over the Japan Sea through the TC season could not be attributed to the direct effect of the reduced SIC in the Bering Sea.

To probe into the possible physical process of the persistent SST cooling in the Japan Sea through the TC season, we examined the surface heat fluxes. This is because if ignoring the effect of surface currents and upper ocean mixing, changes in SST in the ocean would be determined by the net surface heat flux, including the latent heat flux, sensible heat flux, longwave and shortwave radiation fluxes. **Figure 10** shows the regressed four fluxes in the TC season with respect to the negative spring SIC index during 1981–2018, where the positive sign stands for "into the ocean and thus warming" and vice versa. Among the four fluxes in the Japan Sea, the shortwave radiation flux anomalies in response to the spring SIC (**Figure 10D**) displays a similar pattern to the SST anomalies in the Japan Sea. This suggests that the persistent cooling in the Japan Sea through the TC season after its initiation in spring is most likely caused by the reduction of the incoming shortwave radiation reaching the ocean surface. Consistent with the evolution of the regressed SST anomalies (**Figure 6**), the regressed shortwave radiation flux shows negative anomalies in the Japan Sea in spring, which quickly intensifies and extends eastward through the TC season (**Figure 11**). The surface shortwave radiation is largely determined by low clouds in the Japan Sea in summer (e.g., Koseki et al., 2012). The increasing reduction of surface shortwave radiation flux can be attributed to the increasing low cloud cover in the Japan Sea as we can see from the evolution of the regressed low cloud cover with respect to the reduced spring SIC index in **Figure 11**.

The above analysis demonstrates that a positive feedback among low cloud, radiation, and SST (namely the cloud-radiation-SST feedback) could be responsible for the persistent strengthening cooling in the Japan Sea through the TC season triggered by the spring reduced SIC in the Bering Sea. In spring, the anomalous northwesterly associated with the strengthening Aleutian low due to the reduced SIC in the Bering Sea brings

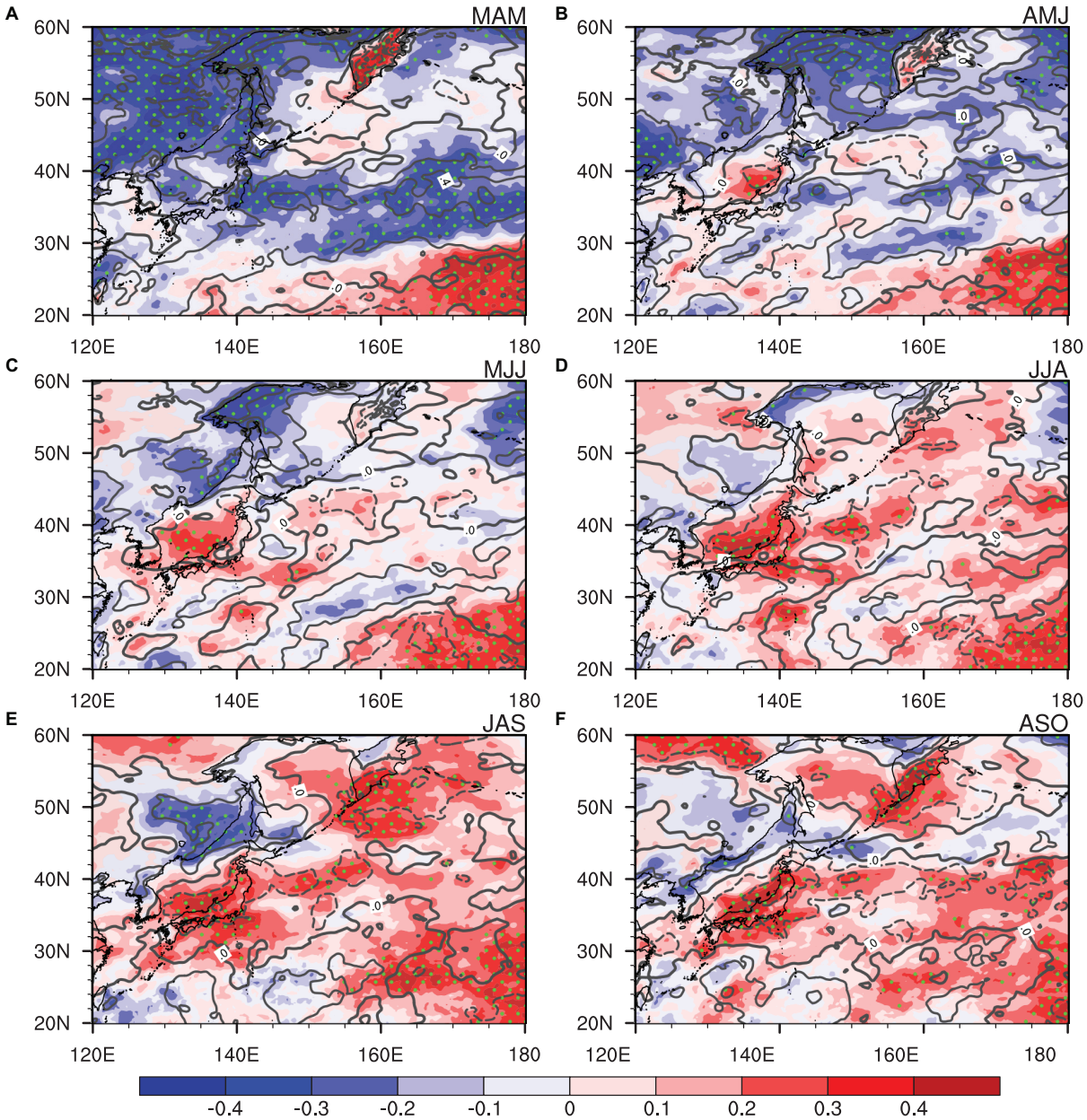

FIGURE 11 | (A-F) Regressed 3-month running averaged low cloud cover (shaded) and shortwave radiation flux (contour; W m^{-2}) from March to October with respect to the negative spring SIC index during 1981–2018. The dotted areas denote where the regressions are statistically significant at 90% confidence level.

dry and cold air to the Japan Sea from the mid-latitude Asian continent. This enhances surface turbulent sensible and latent heat fluxes. Thus, the SST begins to cool down and the boundary layer becomes more stable leading to the formation of low clouds above the Japan Sea and its adjacent regions. Afterwards, the cyclonic anomaly weakens and decays in summer. However, low clouds block the downward short-wave radiation reaching the ocean surface, leading to further cooling of the ocean surface. The strong cooling in turn strengthens the stability of the lower troposphere, which is more favorable for low clouds (Manabe and Strickler, 1964; Lilly, 1968; Moeng, 1986; Klein and Hartmann, 1993; Wang et al., 2004a,b; Koseki et al., 2012). Therefore, through the local positive cloud-radiation-SST feedback process over the Japan Sea and its adjacent regions that the spring SIC anomaly affects the interannual variability of the SWJ, and large-scale circulation and thus the TC activity in the TC season over the WNP. This demonstrates that the spring SST anomaly in the Japan Sea triggered by the SIC anomaly in the Bering Sea plays a key role in bridging the observed relationship between the spring SIC and the ACE in the TC season over the WNP discussed in Section "Results From Statistical and Regression Analyses."

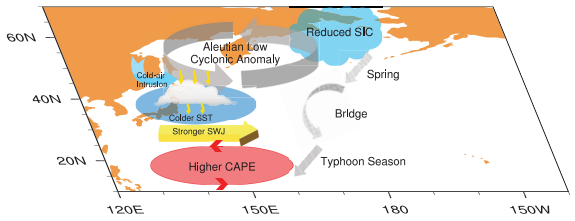

FIGURE 12 | Schematic diagram showing the processes through which the spring SIC affects the WNP environment in the TC season. The reduced SIC induces the intensification and westward shift of the Aleutian low in spring, which increases the low cloud, reduces surface shortwave radiation flux and causes cooling over the Japan Sea. The cloud-radiation-SST feedback intensifies and maintains through the TC season, which leads to the strengthening and southward shift of the SWJ and then induces favorable conditions for TC activity over the WNP. The yellow solid and thick arrow denotes the SWJ, and the yellow solid and thin arrow denotes the surface shortwave radiation flux. The dotted gray arrows indicate the physical process by which the spring SIC anomaly imposes impact in the tropical WNP in the TC season through the bridging role of the cloud-radiation-SST feedback in Japan Sea.

CONCLUSION AND DISCUSSION

This study has documented the negative correlation between the spring SIC in the Bering Sea and the ACE in the TC season over the WNP on the interannual timescale during 1980–2018. The reduced (increased) spring SIC is favorable for higher (lower) ACE, an integrated measure of TC genesis frequency, intensity and tracks. Especially, the spring SIC can greatly affect TC tracks by shifting TC activity meridionally over the WNP. Results from both reanalysis data analysis and atmospheric model experiments demonstrate the key role of the SST anomaly in the Japan Sea in bridging the correlation between the spring SIC and the WNP ACE in the TC season. The associated physical processes are conceptualized in **Figure 12**. In spring, the reduced SIC induces the intensification and westward shift of the Aleutian low, which is consistent with the results in Fan (2007). However, we further pointed out that such changes in the Aleutian low strengthens the cold air intrusion from the mid-latitude Asian continent and induces the cooling and promotes the development of low clouds in the Japan Sea and its adjacent regions. The low clouds reduce the shortwave radiation reaching the ocean surface, further cooling the ocean surface in the Japan Sea. This would in turn increases the stability of the lower troposphere and further enhances the low clouds and thus cools the ocean surface. This local cloud-radiation-SST feedback persistently cools the Japan Sea and the atmosphere above through the TC season, enhancing the meridional gradient of air temperature, leading to the strengthening and southward shift of the SWJ over the East Asia, an anomalous upper-level anticyclone over the WNP, low-level cyclonic circulation anomalies, increased CAPE, and reduced VWS over the tropical WNP. These all are favorable for TC development and intensification and thus the increased ACE over the WNP in the TC season.

Previous studies have revealed the impact of spring sea ice cover in the North Pacific on TC genesis frequency over the WNP (Fan, 2007; Fan and Wang, 2009). Our study focuses on the role of spring SIC in the Bering Sea in contributing to the interannual variability of ACE over the WNP, which includes not only TC genesis frequency, but also TC tracks and intensity. Our results show that the spring SIC has an important impact on the TC tracks and the meridional shift of TC activity over the WNP. Especially, this study reveals the key role of the cloud-radiation-SST feedback in the Japan Sea in bridging the interannual relationship between the spring SIC and the ACE in the TC season over the WNP.

Note that the regressed SST field with respect to the reduced SIC (**Figure 6**) also shows a similar pattern to the second empirical orthogonal function mode (EOF2) of SST anomalies in the North Pacific, namely the Victoria mode (VM), which was highly correlated with TC frequency over the WNP (Pu et al., 2019). However, we found no statistically significant correlation between the summer Victoria mode index and spring SIC index. After the Victoria model signal was removed from the SIC index, the regressed WNP ACE in the TC season with respect to the spring SIC anomaly in the Bering Sea is still significant, suggesting that the impact of the spring SIC is independent of that of the Victoria mode.

Previous studies have also demonstrated a prominent control of ENSO on TC activity over the WNP on interannual time scale (e.g., Camargo and Sobel, 2005; Zhan et al., 2018). We compared the spatial correlations between the Nino3.4 index and WNP ACE in the TC season, and found that the correlation is statistically significant only over the eastern WNP, very different from that associated with the impact of the spring SIC. Therefore, the relative contribution from the spring SIC and ENSO to the interannual variability of TC activity in terms of the ACE might be an interesting topic that deserves a future study. In addition, many studies have shown that Arctic sea ice has been decreasing rapidly (e.g., Serreze and Barry, 2011) and the WNP TC activity has also shown an intensification in recent decades (Emanuel, 2005, 2013; Webster et al., 2005; Park et al., 2017). Our study has revealed a significant negative correlation between the spring SIC and TC ACE in the TC season over the WNP on the interannual time scale. It is unclear whether the rapid decline of the Arctic sea ice has contributed to the intensified TC activity over the WNP. Our study also showed that the spring SIC can greatly affect TC tracks and its meridional shift. It implies that the rapid decline in Arctic sea ice might lead to longer TC tracks and more active TC activity in higher latitudes under a warmer climate. These could be another interesting topic for a future study. Nevertheless, the finding from this study not only has an important implication for seasonal TC forecasts but also suggests a strengthened future TC activity potentially resulting from the rapid decline of Arctic sea ice.

SIGNIFICANCE STATEMENTS

Although many studies have revealed that Arctic sea ice may impose a great impact on the global climate system, including the tropical cyclone genesis frequency over the western North Pacific, it is unknown whether the Arctic sea ice could have any

significant effects on other aspects of TCs, such as TC intensity, lifespan, and track; and if so, what are the involved physical mechanisms. Here, we found that the decreased (increased) spring sea ice in the Bering Sea is favorable (unfavorable) for TC activity, including the mean lifetime of tropical cyclones and the meridional shift of the mean tropical cyclogenesis location and dominant tracks. The spring sea ice anomaly can induce large-scale conditions that significantly affect tropical cyclone activity over the western North Pacific by triggering the cloud-radiation-SST feedback in the Japan Sea. The finding not only has an important implication to seasonal tropical cyclone forecasts but also suggest a strengthened future tropical cyclone activity potentially resulting from the rapid decline of Arctic sea ice.

DATA AVAILABILITY STATEMENT

The original contributions presented in the study are included in the article/supplementary material, further inquiries can be directed to the corresponding author/s.

AUTHOR CONTRIBUTIONS

HF and RZ conceived the study and wrote the manuscript. HF and JZ set and run the numerical experiments. ZW and YW provided critical feedback and helped shape the research and manuscript. All authors contributed to the article and approved the submitted version.

FUNDING

This work has been supported by the National Key Basic Research Project of China (2019YFA0607002), the National Natural Science Foundation of China (Grants 42075015 and 41875114), and the Shanghai Typhoon Research Foundation (TFJJ201919).

ACKNOWLEDGMENTS

The authors are grateful to Drs. Yinao Diao, Chenghu Sun, and Anmin Duan for their constructive comments and suggestions.

REFERENCES

Ashok, K., Guan, Z., and Yamagata, T. A. (2003). A look at the relationship between the ENSO and the Indian Ocean dipole. *J. Meteorol. Soc. Jpn. Ser II* 81, 41–56. doi: 10.2151/jmsj.81.41

Balmaseda, M. A., Ferranti, L., Molteni, F., and Palmer, T. N. (2010). Impact of 2007 and 2008 Arctic ice anomalies on the atmospheric circulation: implications for long-range predictions. *Q. J. R. Meteorol. Soc.* 136, 1655–1664. doi: 10.1002/qj.661

Barnes, E. A. (2013). Revisiting the evidence linking Arctic amplification to extreme weather in midlatitudes. *Geophys. Res. Lett.* 40, 4734–4739. doi: 10.1002/grl.50880

Bell, G. D., Halpert, M. S., Schnell, R. C., Higgins, R. W., Lawrimore, J., Kousky, V. E., et al. (2000). Climate assessment for 1999. *Bull. Am. Meteorol. Soc.* 81, S1–S50.

Bracken, W. E., and Bosart, L. F. (2000). The role of synoptic-scale flow during tropical cyclogenesis over the North Atlantic Ocean. *Mon. Weather Rev.* 128, 353–376. doi: 10.1175/1520-0493(2000)128<0353:trossf>2.0.co;2

Camargo, S. J., and Barnston, A. G. (2009). Experimental dynamical seasonal forecasts of tropical cyclone activity at IRI. *Weather Forecast.* 24, 472–491. doi: 10.1175/2008WAF2007099.1

Camargo, S. J., and Sobel, A. H. (2005). Western North Pacific tropical cyclone intensity and ENSO. *J. Clim.* 18, 2996–3006. doi: 10.1175/JCLI3457.1

Chan, J. C. L. (2005). Interannual and interdecadal variations of tropical cyclone activity over the western North Pacific. *Meteorol. Atmos. Phys.* 89, 143–152. doi: 10.1007/s00703-005-0126-y

Chan, J. C. L., and Liu, K. S. (2004). Global warming and western North Pacific typhoon activity from an observational perspective. *J. Clim.* 17, 4590–4602. doi: 10.1175/3240.1

Chen, G., and Tam, C.-Y. (2010). Different impacts of two kinds of Pacific Ocean warming on tropical cyclone frequency over the western North Pacific. *Geophys. Res. Lett.* 37:L01803. doi: 10.1029/2009GL041708

Chia, H. H., and Ropelewski, C. F. (2002). The interannual variability in the genesis location of tropical cyclones in the Northwest Pacific. *J. Clim.* 15, 2934–2944.

Cowan, L. P., and Hart, R. E. (2020). An objective identification and climatology of upper-tropospheric jets near Atlantic tropical cyclones. *Mon. Weather Rev.* 148, 3015–3036. doi: 10.1175/MWR-D-19-0262.1

Deser, C., and Teng, H. (2008). Evolution of Arctic sea ice concentration trends and the role of atmospheric circulation forcing, 1979–2007. *Geophys. Res. Lett.* 35:L02504. doi: 10.1029/2007GL032023

Du, Y., Yang, L., and Xie, S. (2011). Tropical Indian Ocean influence on Northwest Pacific tropical cyclones in summer following strong El Niño. *J. Clim.* 24, 315–322. doi: 10.1175/2010JCLI3890.1

Emanuel, K. A. (1994). *Atmospheric Convection*. (Oxford: Oxford University Press), 580.

Emanuel, K. A. (2005). Increasing destructiveness of tropical cyclones over the past 30?years. *Nature* 436, 686–688. doi: 10.1038/nature03906

Emanuel, K. A. (2013). Downscaling CMIP5 climate models shows increased tropical cyclone activity over the 21st century. *Proc. Natl. Acad. Sci. U.S.A.* 110, 12219–12224. doi: 10.1073/pnas.1301293110

Fan, K. (2007). North Pacific sea ice cover, a predictor for the Western North Pacific typhoon frequency? *Sci. China Ser. D Earth Sci.* 50, 1251–1257. doi: 10.1007/s11430-007-0076-y

Fan, K., and Wang, H. J. (2009). A new approach to forecasting typhoon frequency over the western North Pacific. *Weather Forecast.* 24, 974–986. doi: 10.1175/2009WAF2222194.1

Fischer, M. S., Tang, B. H., and Corbosiero, K. L. (2017). Assessing the influence of upper-tropospheric troughs on tropical cyclone intensification rates after genesis. *Mon. Weather Rev.* 145, 1295–1313. doi: 10.1175/MWR-D-16-0275.1

Gao, S., Zhu, L., Zhang, W., and Chen, Z. (2018). Strong modulation of the Pacific meridional mode on the occurrence of intense tropical cyclones over the western North Pacific. *J. Clim.* 31, 7739–7749. doi: 10.1175/JCLI-D-17-0833.1

Hersbach, H., Bell, B. D., Berrisford, P., Hirahara, S., Horányi, A., Muñoz-Sabater, J., et al. (2020). The ERA5 global reanalysis. *Q. J. R. Meteorol. Soc.* 146, 1999–2049. doi: 10.1002/qj.3803

Huangfu, J., Chen, W., Huang, R., and Feng, J. (2019). Modulation of the impacts of the Indian Ocean Basin mode on tropical cyclones over the Northwest Pacific during the boreal summer by La Niña Modoki. *J. Clim.* 32, 3313–3326. doi: 10.1175/jcli-d-18-0638.1

Huangfu, J., Huang, R., Chen, W., and Feng, T. (2018). Causes of the active typhoon season in 2016 following a strong El Niño with a comparison to 1998. *Int. J. Climatol.* 38, e1107–e1118. doi: 10.1002/joc.5437

Kim, H., Lee, M., Webster, P. J., Kim, D., and Yoo, J. H. (2013). A physical basis for the probabilistic prediction of the accumulated tropical cyclone kinetic energy in the western North Pacific. *J. Clim.* 26, 7981–7991. doi: 10.1175/JCLI-D-12-00679.1

Klein, S. A., and Hartmann, D. L. (1993). The seasonal cycle of low stratiform clouds. *J. Clim.* 6, 1587–1606. doi: 10.1175/1520-0442(1993)006<1587:tscols>2.0.co;2

Koseki, S., Nakamura, T., Mitsudera, H., and Wang, Y. (2012). Modeling low-level clouds over the Okhotsk Sea in summer: cloud formation and its effects on the Okhotsk high. *J. Geophys. Res. Atmos.* 117, D05208. doi: 10.1029/2011JD016462

Liang, X. Z., and Wang, W. C. (1998). Associations between China monsoon rainfall and tropospheric jets. *Q. J. R. Meteorol. Soc.* 124, 2597–2623. doi: 10.1002/qj.49712455204

Lilly, D. K. (1968). Models of cloud-topped mixed layers under a strong inversion. *Q. J. R. Meteorol. Soc.* 94, 292–309. doi: 10.1002/qj.49709440106

Manabe, S., and Strickler, R. F. (1964). Thermal equilibrium of the atmosphere with a convective adjustment. *J. Atmos. Sci.* 21, 361–385. doi: 10.1175/1520-0469(1964)021<0361:teotaw>2.0.co;2

Moeng, C.-H. (1986). Large-Eddy Simulation of a stratus-topped boundary layer. Part I: structure and budgets. *J. Atmos. Sci.* 43, 2886–2900. doi: 10.1175/1520-0469(1986)043<2886:lesoas>2.0.co;2

Moore, J. T., and Vanknowe, G. E. (1992). The effect of jet-streak curvature on kinematic fields. *Mon. Weather Rev.* 120, 2429–2441. doi: 10.1175/1520-0493(1992)120<2429:teojsc>2.0.co;2

Murakami, H., Li, T., and Hsu, P. (2014). Contributing factors to the recent high level of accumulated cyclone energy (ACE) and power dissipation index (PDI) in the North Atlantic. *J. Clim.* 27, 3023–3034. doi: 10.1175/JCLI-D-13-00 394.1

Nordeng, T. E. (1994). Extended versions of the convective parameterization scheme at ECMWF and their impact on the mean and transient activity of the model in the tropics. *ECMWF Res. Dep. Tech. Memo.* 206, 1–41.

Park, D. S., Ho, C. H., Chan, J., Ha, K.-J., Kim, H.-S., Kim, J., et al. (2017). Asymmetric response of tropical cyclone activity to global warming over the North Atlantic and western North Pacific from CMIP5 model projections. *Sci. Rep.* 7:41354. doi: 10.1038/srep41354

Park, K., Zou, X., and Li, G. (2009). A numerical study on rapid intensification of Hurricane Charley (2004) near landfall. *Front. Earth Sci. China* 3:457. doi: 10.1007/s11707-009-0048-y

Pu, X., Chen, Q., Zhong, Q., Ding, R., and Liu, T. (2019). Influence of the North Pacific Victoria mode on western North Pacific tropical cyclone genesis. *Clim. Dyn.* 52, 245–256. doi: 10.1007/s00382-018-4129-z

Rasmussen, E. N., and Blanchard, D. O. (1998). A baseline climatology of sounding-derived supercell and tornado forecast parameters. *Weather Forecast.* 13, 1148–1164. doi: 10.1175/1520-0434(1998)013<1148:abcosd>2.0.co;2

Rayner, N. A., Parker, D. E., Horton, E. B., Folland, C. K., Alexander, L. V., Rowell, D. P., et al. (2003). Global analyses of sea surface temperature, sea ice, and night marine air temperature since the late nineteenth century. *J. Geophys. Res. Atmos.* 108:4407. doi: 10.1029/2002JD002670

Rinke, A., Dethloff, K., Dorn, W., Handorf, D., and Moore, J. C. (2013). Simulated Arctic atmospheric feedbacks associated with late summer sea ice anomalies. *J. Geophys. Res. Atmos.* 118, 7698–7714. doi: 10.1002/jgrd.50584

Roeckner, E. K., Arpe, L., Bengtsson, L., Christoph, M., Clauseen, L., Dümenil, L., et al. (1996). *The Atmospheric General Circulation Model ECHAM-4: Model Description and Simulation of Present-Day Climate. Max-Planck-Institut für Meteorologie Report Series. 218. Technical Report*. (Hamburg: Max-Planck-Institut für Meteorologie).

Royer, J. F., Planton, S., and Déqué, M. (1990). A sensitivity experiment for the removal of Arctic sea ice with the French spectral general circulation model. *Clim. Dyn.* 5, 1–17. doi: 10.1007/bf00195850

Schneider, T., Bischoff, T., and Plotka, H. (2014). Physics of changes in synoptic midlatitude temperature variability. *J. Clim.* 28, 2312–2331. doi: 10.1175/JCLI-D-14-00632.1

Screen, J. A. (2014). Arctic amplification decreases temperature variance in northern mid- to high-latitudes. *Nat. Clim. Change* 4, 577–582. doi: 10.1038/nclimate2268

Screen, J. A., and Simmonds, I. (2013). Exploring links between Arctic amplification and mid-latitude weather. *Geophys. Res. Lett.* 40, 959–964. doi: 10.1002/grl.50174

Screen, J. A., Simmonds, I., Deser, C., and Tomas, R. (2013). The atmospheric response to three decades of observed Arctic sea ice loss. *J. Clim.* 26, 1230–1248. doi: 10.1175/JCLI-D-12-00063.1

Serreze, M. C., and Barry, R. G. (2011). Processes and impacts of Arctic amplification: a research synthesis. *Glob. Planet. Change* 77, 85–96. doi: 10.1016/j.gloplacha.2011.03.004

Smith, D. M., Dunstone, N. J., Scaife, A. A., Fiedler, E. K., Copsey, D., and Hardiman, S. C. (2017). Atmospheric response to Arctic and Antarctic sea ice: the importance of ocean-atmosphere coupling and the background state. *J. Clim.* 30, 4547–4565. doi: 10.1175/JCLI-D-16-0564.1

Tao, L., Wu, L., Wang, Y., and Yang, J. (2012). Influence of tropical Indian Ocean warming and ENSO on tropical cyclone activity over the western North Pacific. *J. Meteorol. Soc. Jpn. Ser. II* 90, 127–144. doi: 10.2151/jmsj.2012-107

Walsh, J. E. (2014). Intensified warming of the Arctic: causes and impacts on middle latitudes. *Glob. Planet. Change* 117, 52–63. doi: 10.1016/j.gloplacha.2014.03.003

Wang, B., and Chan, J. C. L. (2002). How strong ENSO events affect tropical cyclone activity over the western North Pacific. *J. Clim.* 15, 1643–1658. doi: 10.1175/1520-0442(2002)015<1643:hseeat>2.0.co;2

Wang, Y., Xie, S., Xu, H., and Wang, B. (2004a). Regional model simulations of marine boundary layer clouds over the Southeast Pacific off South America. Part I: control experiment. *Mon. Weather Rev.* 132, 274–296. doi: 10.1175/1520-0493(2004)132<0274:rmsomb>2.0.co;2

Wang, Y., Xu, H., and Xie, S. (2004b). Regional model simulations of marine boundary layer clouds over the Southeast Pacific off South America. Part II: sensitivity experiments. *Mon. Weather Rev.* 132, 2650–2668. doi: 10.1175/MWR2812.1

Webster, P. J., Holland, G. J., Curry, J. A., and Chang, H. R. (2005). Changes in tropical cyclone number, duration, and intensity in a warming environment. *Science* 309, 1844–1846. doi: 10.1126/science.1116448

Weisman, M. L., and Klemp, J. B. (1982). The dependence of numerically simulated convective storms on vertical wind shear and buoyancy. *Mon. Weather Rev.* 110, 504–520. doi: 10.1175/1520-0493(1982)110<0504:tdonsc>2.0.co;2

Woolings, T., Czuchnicki, C., and Franzke, C. (2014). Twentieth century North Atlantic jet variability. *Q. J. R. Meteorol. Soc.* 140, 783–791. doi: 10.1002/qj.2197

Wu, Z., Li, X., Li, Y., and Li, Y. (2016). Potential influence of Arctic Sea Ice to the interannual variations of East Asian spring precipitation. *J. Clim.* 29, 2797–2813. doi: 10.1175/JCLI-D-15-0128.1

Zhan, R., Chen, B., and Ding, Y. (2018). Impacts of SST anomalies in the Indian-Pacific basin on Northwest Pacific tropical cyclone activities during three super El Niño years. *J. Oceanol. Limnol.* 36, 20–32.

Zhan, R., and Wang, Y. (2016). CFSv2-based statistical prediction for seasonal accumulated cyclone energy (ACE) over the western North Pacific. *J. Clim.* 29, 525–541. doi: 10.1175/JCLI-D-15-0059.1

Zhan, R., Wang, Y., and Lei, X. T. (2011a). Contributions of ENSO and East Indian Ocean SSTA to the interannual variability of northwest Pacific tropical cyclone frequency. *J. Clim.* 24, 509–521. doi: 10.1175/2010JCLI3808.1

Zhan, R., Wang, Y., and Wen, M. (2013). The SST gradient between the Southwestern Pacific and the western Pacific warm pool: a new factor controlling the Northwestern Pacific tropical cyclone genesis frequency. *J. Clim.* 26, 2408–2415. doi: 10.1175/JCLI-D-12-00798.1

Zhan, R., Wang, Y., and Wu, C. C. (2011b). Impact of SSTA in the East Indian Ocean on the frequency of northwest Pacific tropical cyclones: a regional atmospheric model study. *J. Clim.* 24, 6227–6242. doi: 10.1175/JCLI-D-10-05014.1

Zhan, R., Wang, Y., and Ying, M. (2012). Seasonal forecasts of tropical cyclone activity over the western North Pacific: a review. *Trop. Cyclone Res. Rev.* 1, 307–324. doi: 10.6057/2012TCRR03.07

Zhang, W., Vecchi, G. A., Murakami, H., Villarini, G., and Jia, L. (2015). The Pacific Meridional Mode and the occurrence of tropical cyclones in the western North Pacific. *J. Clim.* 29, 381–398. doi: 10.1175/JCLI-D-15-0282.1

Zhao, G., Huang, G., Wu, R., Tao, W., Gong, H., Qu, X., et al. (2015). A new upper-level circulation index for the East Asian summer monsoon variability. *J. Clim.* 28, 9977–9996. doi: 10.1175/JCLI-D15-0272.1

Zhao, H., Wu, L., and Zhou, W. (2011). Interannual changes of tropical cyclone intensity in the western North Pacific. *J. Meteorol. Soc. Jpn. Ser. II* 89, 243–253. doi: 10.2151/jmsj.2011-305

Conflict of Interest: The authors declare that the research was conducted in the absence of any commercial or financial relationships that could be construed as a potential conflict of interest.